Available online at www.sciencedirect.com
ScienceDirect
Polymer 48 (2007) 4143–4151
polymer
www.elsevier.com/locate/polymer

Poly(*p*-phenylenesulfide)-based nano-composite formation: Delamination of organically modified layered filler via solid-state processing

Tomotaka Saito [a], Masami Okamoto [a,*], Ryoichi Hiroi [b], Minoru Yamamoto [b], Takashi Shiroi [b]

[a] *Advanced Polymeric Nanostructured Materials Engineering, Graduate School of Engineering, Toyota Technological Institute, Hisakata 2-12-1, Tempaku, Nagoya 468-8511, Japan*

[b] *Advanced Material Products Group, Research and Technical Center, Otsuka Chemicals Co. Ltd., Kagasuno Kawauchi-Cho 463, Tokushima 771-0193, Japan*

Received 15 February 2007; received in revised form 1 May 2007; accepted 1 May 2007
Available online 13 May 2007

Abstract

Solid-state processing for the preparation of poly(*p*-phenylenesulfide) (PPS)-based nano-composites having finely dispersed layered fillers was conducted. The mixture of PPS and organically modified layered filler (OMLF) (95:5 wt./wt.) was subjected to the processing using thermostatted hot-press at ambient temperature and 150 °C, below T_m of PPS (i.e., PPS is still at the solid-state), and applying pressures of 7, 14 and 33 MPa for 30 s. The mixture exhibited disorder and delaminated layer structure with the thickness of 40–80 nm into PPS matrix. On the contrary, nano-composite prepared by melt compounding at 300 °C for 3 min showed the large stacked silicate layers in the PPS matrix. The solid-state processing led to delamination of the silicate layers and attained the discrete dispersion.

Keywords: Delamination; Solid-state processing; Layered fillers

1. Introduction

A significant amount of work has already been done on various aspects of polymeric nano-composite containing organically modified layered fillers (OMLFs) [1]. However, complete exfoliation of OMLFs in continuous polymer matrix is still challenging issue because it could not be satisfactorily attained. We know, by now, that the complete exfoliation is not feasible after melt intercalation with appropriate shear. Delamination of stacked layered fillers in polymeric nano-composite is the ultimate target for controlling better overall materials' properties. Thus, we are far from the goal of understanding the mechanisms of the nano-structure control and the preparation of the nano-composite with discrete dispersion of the nano-fillers. From this reason, a novel preparation method is currently in progress.

The effect of the supercritical CO_2 (sc-CO_2) fed to the tandem extruder on the dispersion of organically modified montmorillonite (MMT) with different intercalants into nylon 6 matrix was examined [2]. In the absence of sc-CO_2, pressure improved the MMT-clay delamination by reducing the free volume of the polymer and increasing the interaction between chains and ultimately increasing the viscosity. Using sc-CO_2 did not improve the clay dispersion due to the decreasing the melt viscosity.

Another interesting approach for the delamination of OMLFs is an ultrasound in the preparation of nano-composites. The effect of the *in situ* ultrasound on the polymer/MMT melt phase is reported [3]. An effective method to enhance the dispersion, intercalation and exfoliation of OMLFs in thermoplastic-based nano-composites is reported. The same experiment was done in another report for polypropylene (PP)-base nano-composite preparation [4]. The maximum power output and frequency of the ultrasonic generator are 300 W and 20 kHz, respectively. They described the fine dispersion of silicate layers in PP matrix after ultrasonic treatment (100 W). However, the

* Corresponding author. Fax: +81 (0)52 809 1864.
E-mail address: okamoto@toyota-ti.ac.jp (M. Okamoto).

0032-3861/$ - see front matter © 2007 Elsevier Ltd. All rights reserved.
doi:10.1016/j.polymer.2007.05.014

ultrasonic oscillations exhibited a little effect on the delamination of OMLFs as revealed by transmission electron microscope (TEM) observation. Thus, the compounding with an assist from sc-CO_2 fluids and ultra-sonication did not improve the state of the nano-filler dispersion once a critical morphology was established. That is, the dispersion of the nano-filler in the polymer matrix is governed by judicious choice of OMLF.

In this regard, we also reported that an optimal interlayer structure on OMLF is most favorable for nano-composite formation with respect to the number per area and size of surfactant (intercalant) chains [5]. The shear stress has little effect on the delamination of the layer as compared with the optimal interlayer structure on OMLF [6]. This reasoning is consistent with the intercalated structure reported by so many nano-composite researchers, who can prepare only intercalated (not exfoliated) nano-composites via simple melt extrusion technique [1].

Although the intercalation technology of the polymer melt is developed along with the current industrial process, such as extrusion and injection molding, we have to develop more innovative compounding process, especially in the preparation of the nano-composites possessing discrete dispersion of the nano-fillers.

Very recently, Wang et al. [7] reported the exfoliation of talc fillers by solid-state shear processing using pan-type mill, to prepare PP/talc nano-composites. Although the delamination of talc fillers was not achieved in the nano-composite as revealed by TEM images, no indication of the layer correlation was observed in wide-angle X-ray diffraction (WAXD). The solid-state shear processing may be an innovative technique to delaminate the layered fillers in overcoming the pressure drop (Δp) within the nano-galleries. Because Δp within the nano-galleries makes the polymer penetration more difficult and provides the formation of intercalated structure (coherent order of the layers) without delamination [5,8] (Appendix A).

In this paper, we challenge solid-state processing to delaminate the stacked, layered filler in the polymer matrix. We report a novel method for the nanoscale control of the dispersed layered fillers.

2. Experimental

OMLF used in this study was synthetic fluorine hectorite (*syn*-FH) intercalated with *n*-hexadecyl tri-*n*-butyl phosphonium ($C_{16}TBP^+$) cation. The alkylphosphonium cation as an intercalant has an advantage for the thermal stability than alkylammonium one [8,9]. A poly(*p*-phenylenesulfide) (PPS) *fine* powder ($M_n = 1.0 \times 10^4$ g/mol, $T_m = 285$ °C and average particle size = 10 μm), purchased from Aldrich, was used as a polymer matrix. The homogeneous mixture of PPS and OMLF in the weight ratio 95:5 was prepared. We conducted the solid-state processing using thermostatted hot-press (Techno Supply Co.). The mixtures were subjected to a hot-press at ambient temperature (~25 °C) and 150 °C for 30 s, varying applied pressures of 7, 14 and 33 MPa. In the solid-state processing, the pressure was removed and again applied for 30 s and procedure was repeated for 15 times. Since the

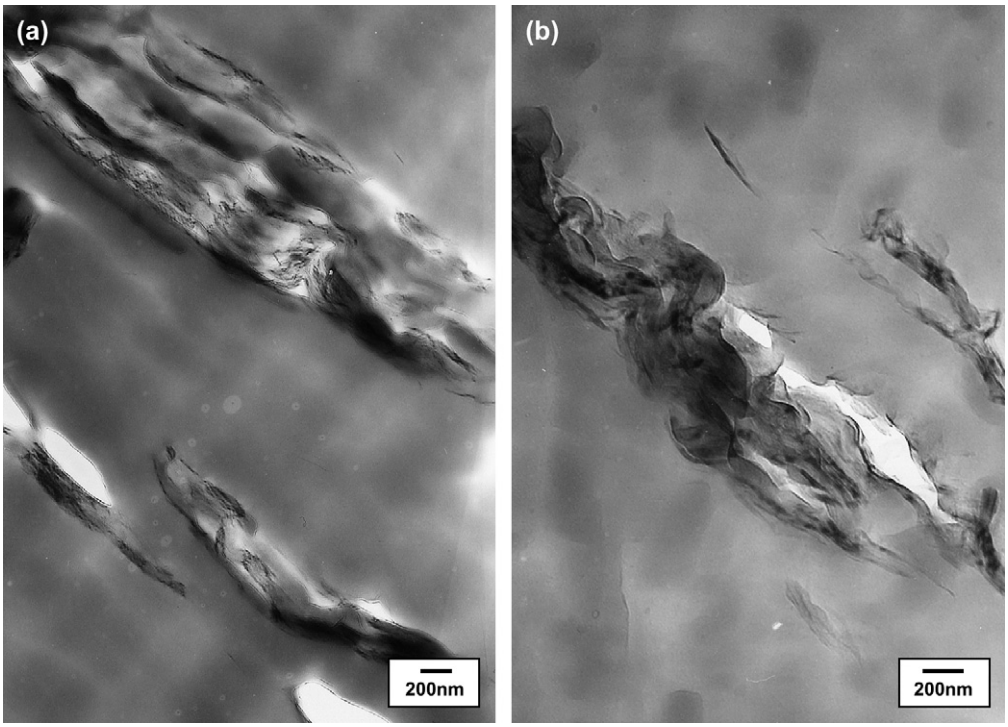

Fig. 1. Bright filed TEM images of (a) PPS/*syn*-FH-$C_{16}TBP^+$ (95:5 wt./wt.) mixture before solid-state processing. The samples are prepared by annealing at 300 °C for 30 s (without shear processing), and (b) PPS/*syn*-FH-$C_{16}TBP^+$ prepared by melt compounding with shear (operated at 300 °C for 3 min). The dark entities are the crosssection and/or face of intercalated-and-stacked silicate layers, and the bright areas are the matrix.

melting temperature of the intercalant ($C_{16}TBP^+$) into the nano-galleries was −23.5 °C, we can observe the effect of layer delamination at each temperature. The recovered sheet was about 1 mm thickness and was kept at room temperature prior to the measurements.

The nano-structure analyses of wide-angle X-ray diffraction (WAXD) and transmission electron microscopy (TEM) were carried out using the same apparatus as in the previous articles [10,11]. To investigate the micro-scale morphology of the nano-composites, we also used polarizing optical microscope (POM). Because TEM micrograph cover a small area, which might not be an entire representative for the overall microstructure of the sample. The recovered sheets were first sandwiched between two pieces of cover glass and placed on a laboratory hot plate at above T_m of PPS for 30 s. The molten film was then rapidly put on a thermostatted hot-stage (300 °C) (Linkam RTVMS, Linkam Scientific Instruments, Ltd.) mounted on a POM (Nikon OPTIPHOTO2-POL). For analyzing the features of the micrographs, we carried out fast Fourier transform (FFT) analysis on digitally saved images of POM micrographs using the commercial image analysis software (Ultimage®, Graftek, France) [12], which allowed to provide us information equivalent to the scattering analyses.

For comparison, the PPS-based nano-composite preparation was conducted via conventional melt compounding operated at 300 °C for 3 min [6]. The extruded samples were dried under vacuum at 120 °C for 6 h to remove water. The dried nano-composite was then converted into sheets with a thickness of 0.7–2 mm by pressing with ≈1.5 MPa at 300 °C for 1 min using a hot-press.

3. Results and discussion

3.1. PPS-based nano-composites formation with or without shear compounding

We conducted nano-composite preparation with or without shear processing. Fig. 1(a) shows TEM image of PPS-based nano-composites prepared by annealing at 300 °C for 30 s (without shear processing). That is, this sample is an unprocessed mixture of PPS and OMLF just before solid-state processing. It is clear from the TEM image that stacked-and-agglomerated structure of layers is evident in PPS/*syn*-FH-$C_{16}TBP^+$ system. The large agglomerated tactoids of about 300 nm thickness are seen in Fig. 1(a). Fig. 1(b) shows the results of the nano-composite prepared by melt compounding with shear (operated at 300 °C for 3 min). For PPS/*syn*-FH-$C_{16}TBP^+$, we still observe large stacked silicate layers in the nano-composite. Despite shear processing at 300 °C, the nano-composite exhibits some staked-and-flocculated silicate layers in the PPS matrix [6]. On the other hand, when we use MMT intercalated with $C_{16}TBP^+$, a more homogeneously and finely dispersed layer structure is developed in PPS/MMT-$C_{16}TBP^+$ system, with and without shear processing (data not shown) [6]. This indicates that the OMLFs having lower surface charge density (ζ) (i.e., MMT ($\zeta = 0.780\ e^-/nm^2$) rather than *syn*-FH ($\zeta = 0.971\ e^-/nm^2$)) leads to a lower coherent order of the layer structure and the layer structure is presumably destroyed when the OMLFs are modified by some intercalant, which is miscible with polymer matrix.

3.2. PPS-based nano-composite formation via solid-state processing

3.2.1. Variation of WAXD profiles

WAXD patterns, in the range of diffraction angle $2\Theta = 1-10°$, for the typical examples of nano-filler powders are presented in Fig. 2(a). The mean interlayer spacing of the (001) plane ($d_{(001)}$) for the *syn*-FH that was modified by $C_{16}TBP^+$ [*syn*-FH-$C_{16}TBP^+$] obtained by WAXD measurements is 2.741 nm ($2\Theta = 3.22°$). The appearances of small peaks observed at $2\Theta = 7.60°$ and 11.36° were confirmed that these reflections are due to (002) and (003) planes of *syn*-FH-$C_{16}TBP^+$. *syn*-FH-$C_{16}TBP^+$ exhibits well-ordered layered structure proved by WAXD with diffraction maxima up to the third order. Fig. 2(b) shows the result of the mixture of PPS and *syn*-FH-$C_{16}TBP^+$ (95:5 wt./wt.). The intensity of the WAXD peaks is decreased sharply due to the diluent effect. On the contrary, after solid-state processing with applying pressure of 33 MPa at 150 °C, the WAXD pattern of the

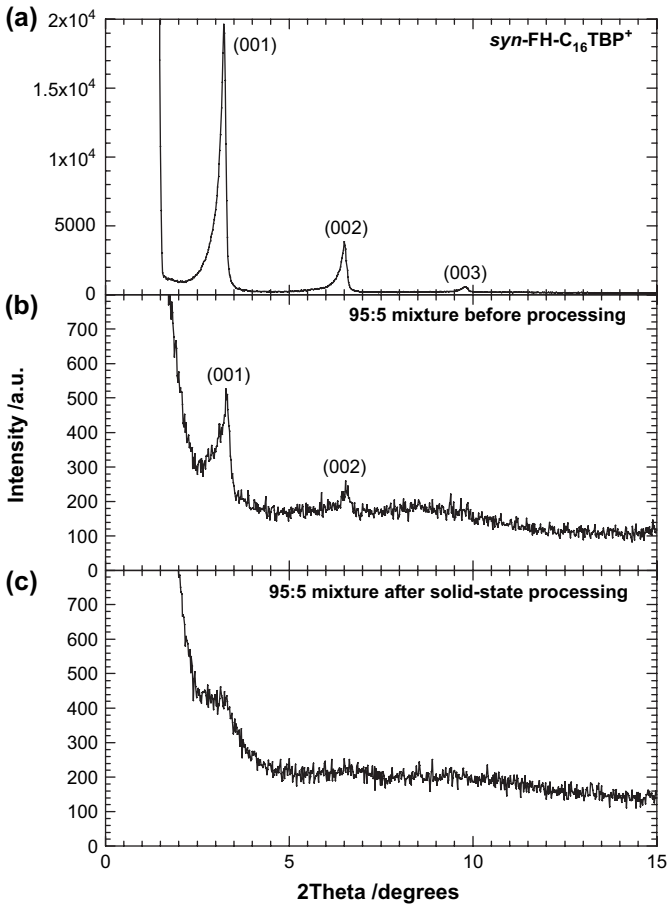

Fig. 2. WAXD patterns of (a) *syn*-FH-$C_{16}TBP^+$, (b) mixture of PPS and *syn*-FH-$C_{16}TBP^+$ (95:5 wt./wt.) before solid-state processing and (c) processed mixture of PPS and *syn*-FH-$C_{16}TBP^+$ (95:5 wt./wt.) with applying pressure of 33 MPa at 150 °C.

mixture is almost featureless diffraction, only exhibiting a broad and weak reflection (Fig. 2(c)), possibly because of the layer disorder or collapse of the layer structure. The silicate concentration does not contribute to the featureless diffraction because of the comparison with Fig. 2(b).

In Fig. 3, the whole view of the WAXD patterns just after solid-state processing was presented. For all processed samples, the intensity of the (001) plane of the *syn*-FH-$C_{16}TBP^+$ decreases with loading pressure. For the samples with applying pressure of 33 MPa, the WAXD pattern of the mixture is almost a featureless diffraction as mentioned before, only exhibiting an orthorhombic unit cell of the crystallized PPS [13]. The diffraction peaks at $2\Theta = 19.0°$, 20.5°, 25.5° and 27.5° correspond to the planes of (110), (111/200), (112) and (211), respectively. The significant difference in the WAXD profiles among the processing condition is not observed.

Fig. 4 exhibits WAXD patterns for the typical examples of both processed and unprocessed mixtures after annealing at 300 °C for 30 s (without shear stress). The profiles were taken at room temperature. We can see a large effect of the processing on the collapse of the layer structure of OMLF. After annealing, the disappearance of sharp Bragg peaks [(001) and (002) planes] in OMLFs clearly indicates the dispersed

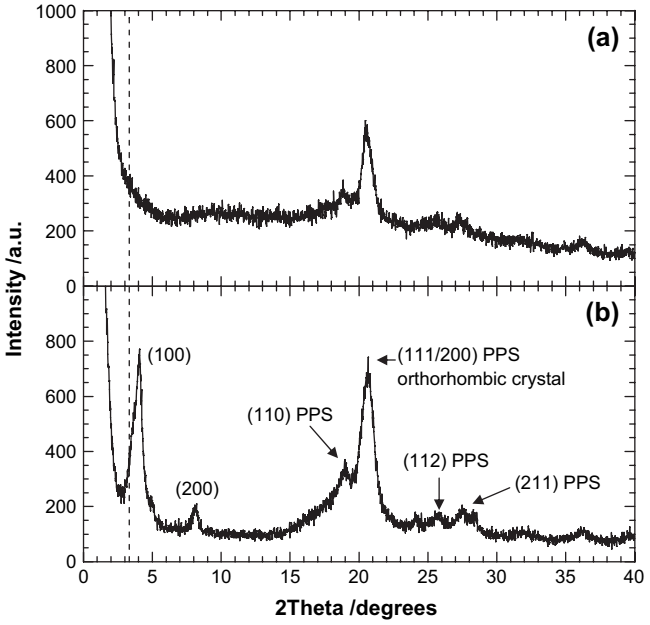

Fig. 4. WAXD patterns after annealing at 300 °C for 30 s: (a) solid-state processed mixture with applying pressure of 33 MPa at 150 °C and (b) unprocessed mixture. All profiles were taken at room temperature. The dashed line in each figure indicates the location of silicate (001) reflection of each OMLF. The strong diffraction peaks at $2\Theta = 15–30°$ are assigned to the orthorhombic crystal of PPS.

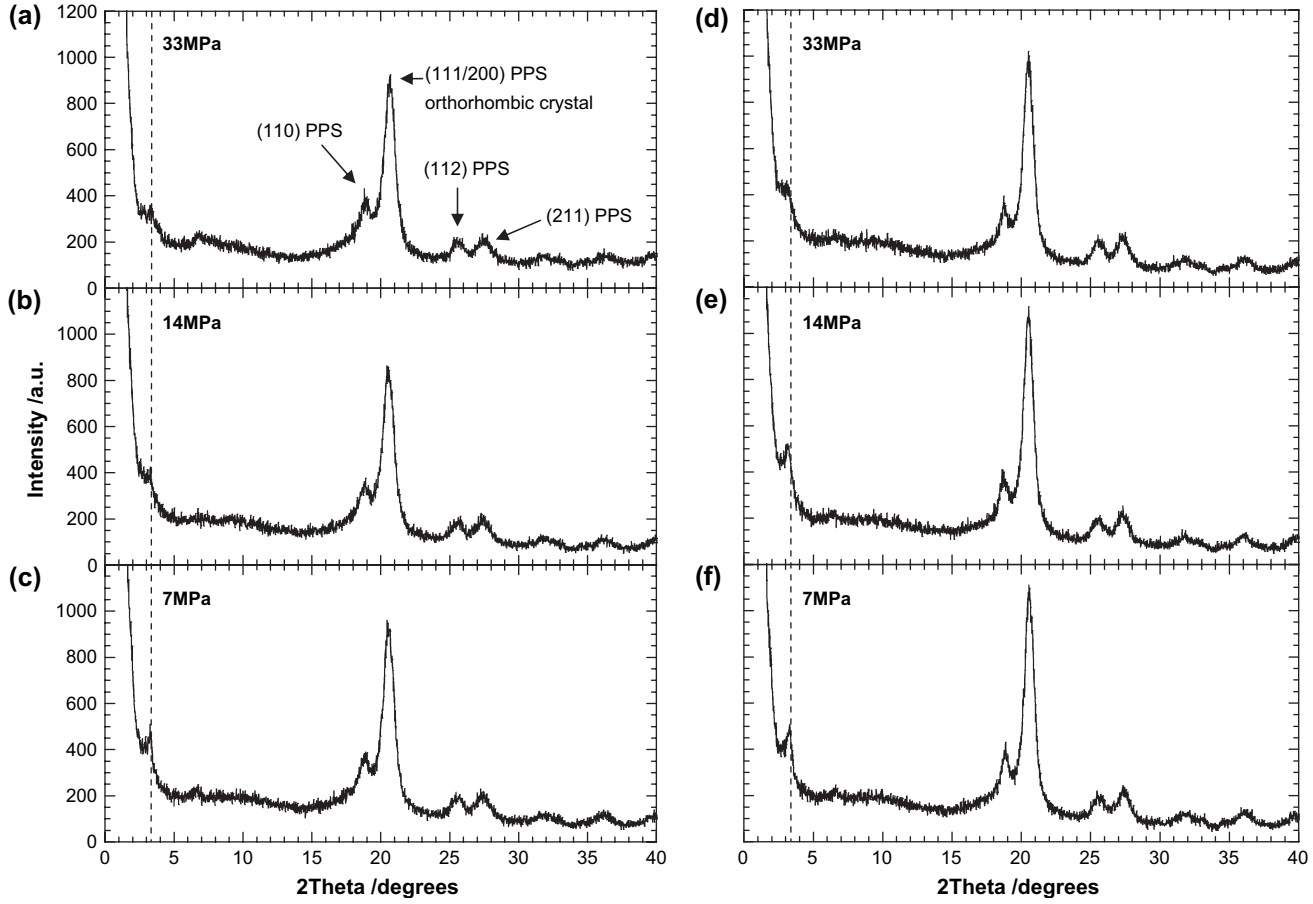

Fig. 3. WAXD patterns for solid-state processed mixtures with applying pressure of (a) 33 MPa at room temperature (r.t.), (b) 14 MPa at r.t., (c) 7 MPa at r.t., (d) 33 MPa at 150 °C, (e) 14 MPa at 150 °C, and (f) 7 MPa at 150 °C. The dashed lines in each figure are the (001) peak position of *syn*-FH-$C_{16}TBP^+$ before solid-state processing. The strong diffraction peaks at $2\Theta = 15–30°$ are assigned to the orthorhombic crystal of PPS.

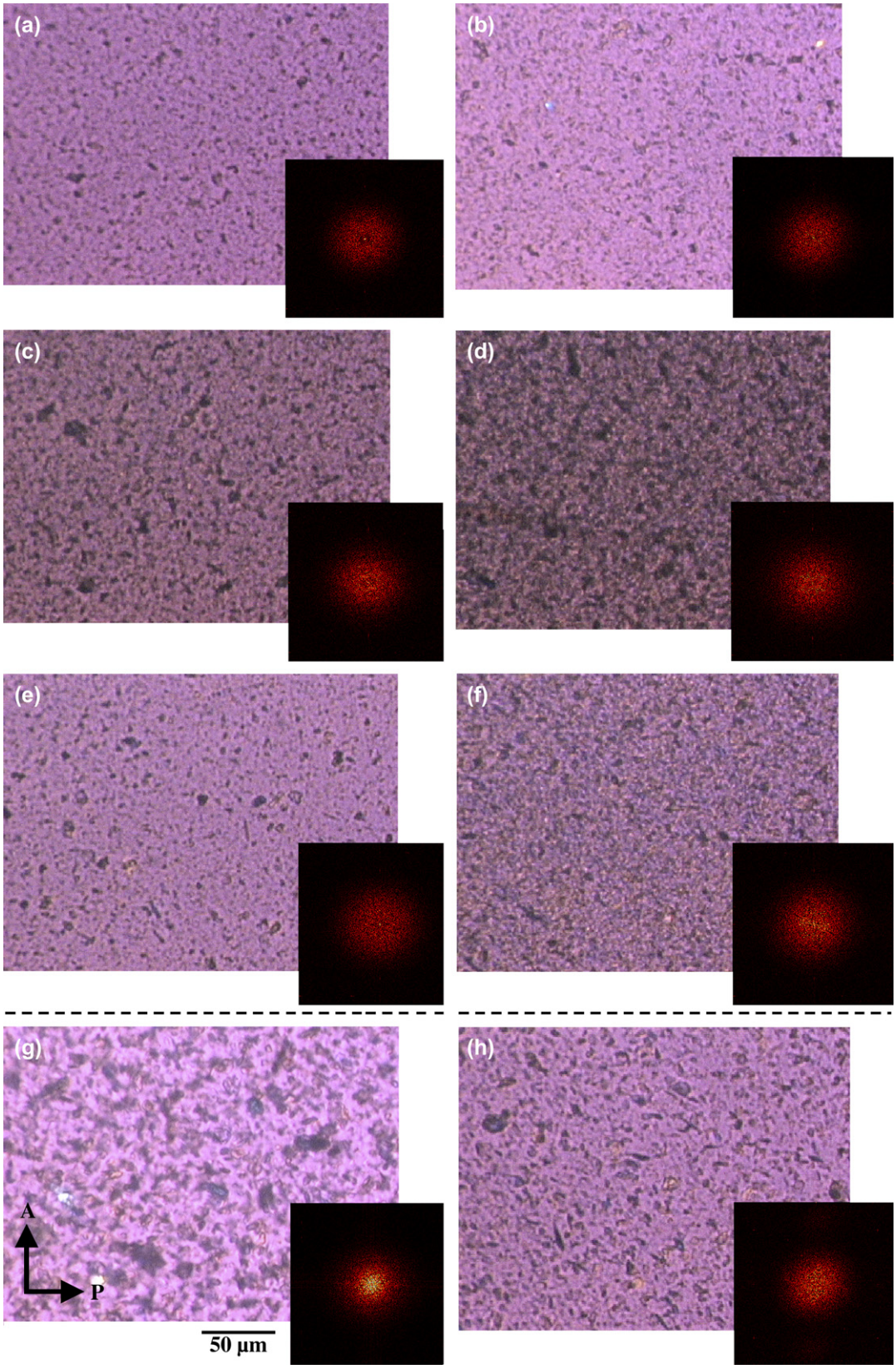

Fig. 5. Polarized optical micrographs for solid-state processed mixtures with applying pressure of (a) 33 MPa at room temperature (r.t.), (b) 14 MPa at r.t., (c) 7 MPa at r.t., (d) 33 MPa at 150 °C, (e) 14 MPa at 150 °C, and (f) 7 MPa at 150 °C. Micrographs of (g) a mixture before solid-state processing and (h) a mixture prepared by melt compounding with shear. All micrographs were taken at 300 °C just after annealing for 30 s (without shear processing). The inset in each picture is a computed FFT spectrum of the micrograph.

behavior of the silicate layers in the PPS matrix (Fig. 4(a)). We confirmed that this behavior is essentially the same at any other processed mixtures. In the case of the unprocessed mixture corresponding to the TEM image of Fig. 1(a), the interlayer shrinkage takes place after annealing without the thermal decomposition of the intercalant (Fig. 4(b)) [8]. The apparent interlayer expansion/shrinkage was deeply discussed in our previous articles [5,6,8]. Such discussion is beyond the objects of this paper.

It is interesting to note the disappearance of the peaks after annealing at 300 °C. For explaining this remarkable difference of the profiles (cf. Fig. 3(d) versus Fig. 4(a)), we speculate the large layer slippage takes place during processing due to the lubrication between the two platelets, where the intercalants are in liquid state. With decreasing the value of R by mechanical approach, the reduction of the attractive force, accompanying the polymer penetration into the nano-galleries and leading to a high level of the dispersion of the OMLF is expected (Appendix A). This discussion is further supported by the morphology observation.

3.2.2. Morphology

To elucidate the morphologies before and after solid-state processing, we conducted POM observation at 300 °C.

Fig. 5 shows the POM photographs with their FFT patterns of the mixtures prepared by annealing at 300 °C for 30 s (without shear processing). It is clear from the POM photographs that stacked-and-agglomerated structure of layers is evident

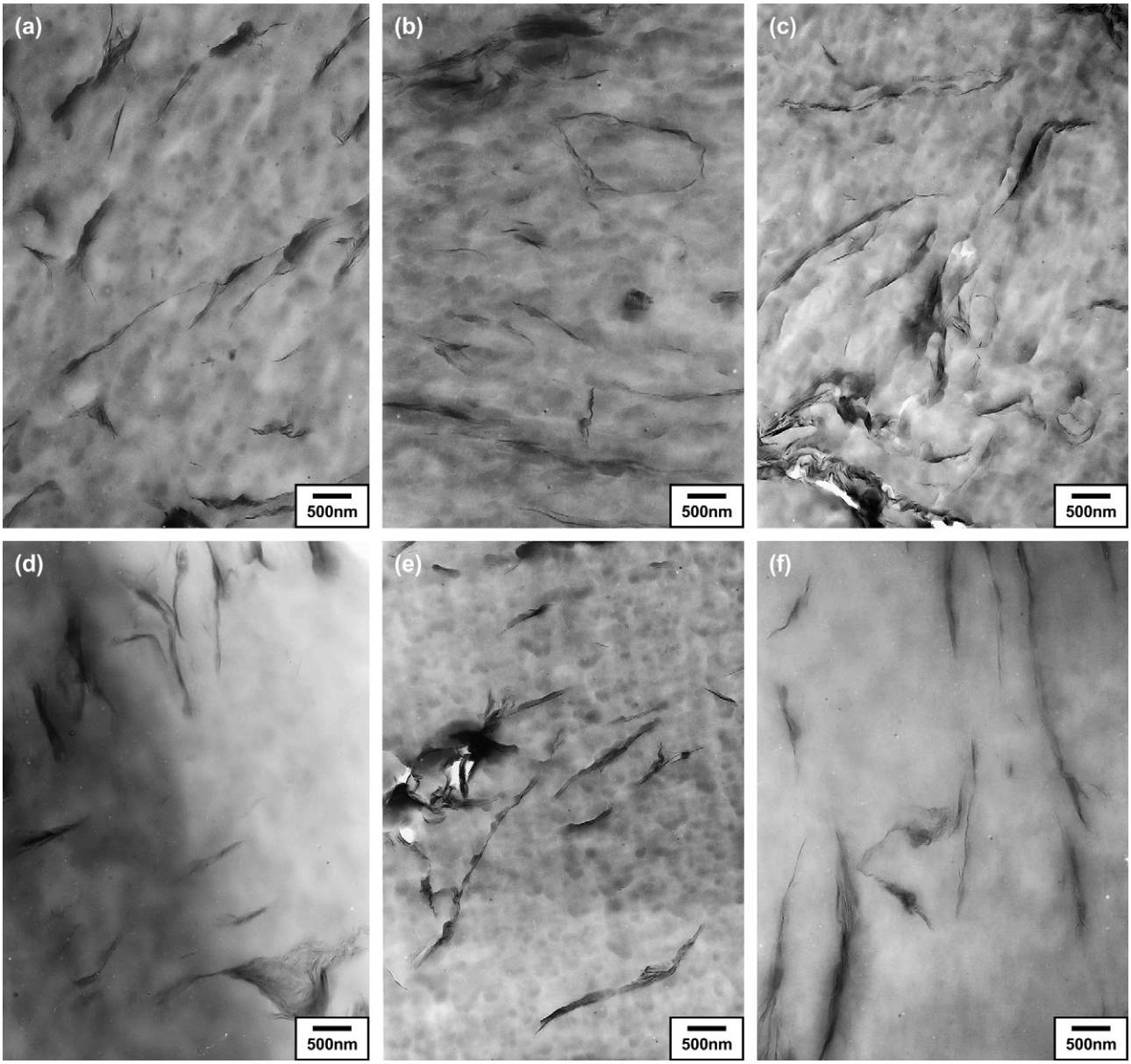

Fig. 6. Bright field TEM images of samples after solid-state processed mixture with applying pressure of (a) 33 MPa at room temperature (r.t.), (b) 14 MPa at r.t., (c) 7 MPa at r.t., (d) 33 MPa at 150 °C, (e) 14 MPa at 150 °C, and (f) 7 MPa at 150 °C. All samples are prepared by annealing at 300 °C for 30 s (without shear processing). The dark entities are crosssection and/or face of intercalated-and-stacked silicate layers, and the bright areas are the matrix.

in the unprocessed mixture (Fig. 5(g)) and melt compounded sample (Fig. 5(h)), whereas a good dispersion appears in the processed sample (Fig. 5(a)–(f)). The FFT pattern shows weak scattering with isotropy (halo) compared with that of the unprocessed mixture. This indicates that the particles size of the dispersed nano-filler becomes smaller during solid-state processing. There is no significant difference in the FFT patterns between processing temperatures. For high applying pressure (33 MPa), however, the FFT patterns exhibits more weak scattering feature compared with that of low pressure condition (7 MPa). The dispersion state in the nanometer scale was directly observed via TEM analyses.

Fig. 6 shows the results of TEM bright field images of the mixtures corresponding to the POM experiments, in which dark entities are the crosssection of layered nano-fillers. The disorder and delaminated silicate layer structures with the thickness of 40–80 nm are observed in each TEM image compared with unprocessed or melt compounded sample (cf. Fig. 1(a) and (b)). This is a unique observation of the discrete silicate layers. We estimated the form factors obtained from TEM images, i.e. average value of the particle length (L), thickness (D) of the dispersed particles and the correlation length (ξ) between the particles. The details of the evaluation were described in our previous paper [11]. The results are presented in Table 1. The values of L are estimated by the limitation of the area of the micrograph due to the magnification factor. Therefore, these values are not so significant compared with that of D. However, the dispersed structure of layered fillers having extremely large value of L is evident in the large layer slippage. For processing at 150 °C the D value decreases with decreasing applying pressure, while at low temperature condition (~25 °C) the value exhibits opposite trend with applying pressure. The intercalants into nano-galleries act as a lubricant at processing temperature. Above the glass transition temperature of matrix PPS ($T_g = \sim 80$ °C), the solid-state processing provides small effect because of the softening of PPS compared with low temperature condition (~25 °C). The adaptive temperature protocol for the processing might be above T_m of the intercalants and below T_g of the matrix polymer. Therefore, the applying pressure might be more important factor than the processing temperature at low temperature condition.

From these facts, the solid-state processing is extremely effective method to collapse the stacked structure. This processing leads to the layer delamination accompanying the discrete dispersion.

Table 1
Form factors of PPS-based nano-composites prepared via solid-state processing with various conditions

Temperature	Parameters	33 MPa	14 MPa	7 MPa
150 °C	L/nm	1340[a]	1250[a]	1300[a]
	D/nm	97 ± 10	72 ± 10	69 ± 10
	ξ/nm	784 ± 100	725 ± 100	632 ± 100
Room temperature	L/nm	1120[a]	1340[a]	860[a]
	D/nm	45 ± 10	47 ± 10	78 ± 10
	ξ/nm	760 ± 100	770 ± 100	620 ± 100

[a] Some nano-fillers have large value of L (greater than 2 μm).

4. Conclusions

We have described a novel and economic method for the nanoscale control of the dispersed layered fillers via solid-state processing. The effect of the different temperatures and applying pressures on the delaminating behavior of the nano-fillers was examined. This processing led to delaminate of the silicate layers and attained the discrete dispersion. This approach can be extended to prepare polymeric nano-composites with delamination of the nano-fillers in overcoming the pressure drop within the nano-galleries. In this study, the applying pressure might be more important factor than the processing temperature at low temperature condition (below T_g of PPS).

Acknowledgment

This work was supported by the MEXT "Collaboration with Local Communities" Project (2005–2009).

Appendix A

The pressure drop difference (Δp) into the nano-galleries is generated by the liquids having large surface tension into two platelets [14]. Δp is given by

$$\Delta p = \gamma\left(\frac{1}{R} - \frac{\cos\,\theta}{H/2}\right) \tag{A1}$$

where γ is the surface tension of the intercalant, R is the radius of the disk if we assume all platelets are of identical disk form, θ is the contact angle (<90°), and H is the distance between two disks, corresponding to the interlayer opening. When the value of H is much smaller than the value of R, i.e. nano-gallery, the value of Δp become negative, suggesting that the attractive force is generated between two disks. The attractive force F is defined as [14]

$$F = \pi R^2 \Delta p + 2\pi R\gamma \sin\,\theta \tag{A2}$$

We consider here Δp in order to prove the validity of the above model in case of the melt intercalation, with value of γ is 50 mN/m (average value of H_2O and $C_{18}H_{38}$), R is 50 nm, H is 2 nm (≅ final interlayer opening [5,6,8]), and θ is less than 90° because the intercalant wets the layer surface fully due to presumably the attractive interaction between negative charges of the layers and alkylammonium or alkylphosphonium cations. Therefore, the calculated value of Δp is equal to −24 MPa ($F = 1.7 \times 10^{-7}$ N) by assuming θ as 60°. This value is quite larger compared to that of atmospheric pressure (≅0.1 MPa). This pressure difference may make the polymer penetration more difficult and provides a good balance between the polymer penetration (interlayer expansion)

and formation of intercalated structure (coherent order of the layers).

The above discussion further supports the observation of the limited value of the final interlayer opening (Appendix B). Furthermore, this pressure difference should be compared to the shear stress during melt compounding. In case of the preparation of poly(L-lactide) (PLA)-based nano-composites, the shear stress (~0.1 MPa at 175 °C [15]) is much lower than the pressure difference (~−24 MPa), suggesting the shear stress have little effect on the delamination (exfoliation) of the layers. This reasoning is consistent with the intercalated structure reported by so many nano-composite researchers, who can prepare only intercalated (not exfoliated) nano-composites via simple melt extrusion technique [1].

Appendix B

Figs. 7 and 8 summarize the layer expansion after preparation of various nano-composites, i.e. initial layer opening, layer expansion (after subtraction of the initial layer opening), and final layer opening. All nano-composites in the figures were prepared by melt compounding operated at 150 °C for poly(butylene succinate) (PBS) [16,17], 190 °C for poly(vinylidene fluoride) (PVDF) [18], 200 °C for PP [19], 210 °C for PLA [20,21], 240 °C for sulfonated poly(ethylene terephthalate) copolymer (PES) [8], 240 °C for poly[styrene-*co*-(maleic anhydride)] (PSMA) [22] and 300 °C for PPS [23].

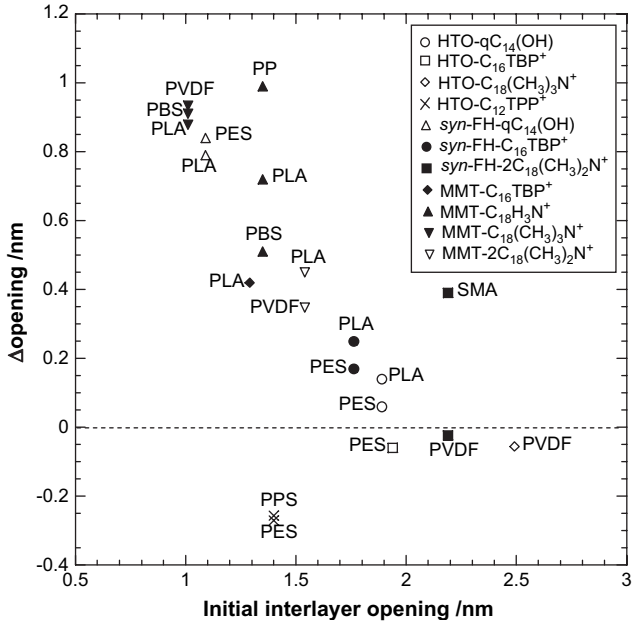

Fig. 7. Plot of initial interlayer opening versus Δ opening for various OMLFs intercalated with poly(butylene succinate) (PBS), poly(vinylidene fluoride) (PVDF), polypropylene (PP), poly(L-lactide) (PLA), sulfonated poly(ethylene terephthalate) copolymer (PES), poly[styrene-*co*-(maleic anhydride)] (PSMA) and PPS after melt intercalation. Layered titanate (HTO), *syn*-FH and MMT are intercalated with various intercalants; e.g., *N*-(cocoalkyl)-*N*,*N*-[bis(2-hydroxyethyl)]-*N*-methyl ammonium ($qC_{14}(OH)$), octadecylammonium ($C_{18}H_3N^+$), octadecyl tri-methylammonium ($C_{18}(CH_3)_3N^+$), dioctadecyldimethylammonium ($2C_{18}(CH_3)_2N^+$), and *n*-octyl tri-phenyl phosphonium cations ($C_{12}TPP^+$).

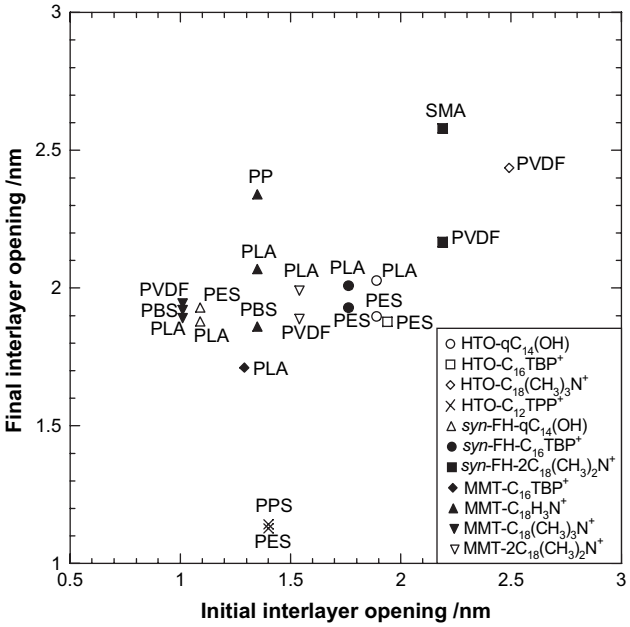

Fig. 8. Plot of initial interlayer opening versus final layer opening for various OMLFs after preparation of nano-composites.

An interesting feature in the polymer melt intercalation into the nano-galleries is the final interlayer opening. As seen in Fig. 7, the interlayer expansion (= Δ opening) depends on the initial interlayer opening after melt intercalation. The smaller initial opening leads to the larger interlayer expansion. The intercalation of polymer chains takes place successfully, regardless of the polymer matrices, the miscibility between polymer and intercalants, and Lewis-acid strength of the intercalants [6]. At the same time, the smaller initial opening gives almost same final interlayer opening (≅1.8–2.2 nm) (Fig. 8). In other words, the final interlayer opening does not depend on the initial opening.

References

[1] Sinha Ray S, Okamoto M. Prog Polym Sci 2003;28:1539.
[2] Yang K, Ozisik R. Polymer 2006;47:2849.
[3] Lee EC, Mielewski DF, Baird RJ. Polym Eng Sci 2004;44:1773.
[4] Zhao L, Li J, Guo S, Du Q. Polymer 2006;47:2460.
[5] Yoshida O, Okamoto M. Macromol Rapid Commun 2006;27:751.
[6] Saito T, Okamoto M, Hiroi R, Yamamoto M, Shiroi T. Macromol Mater Eng 2006;291:1367.
[7] Shao W, Wang Q, Li K. Polym Eng Sci 2005;45:451.
[8] Yoshida O, Okamoto M. J Polym Eng 2006;26:919.
[9] Maiti P, Okamoto M, Yamada K, Ueda K, Okamoto K. Chem Mater 2002;14:4654.
[10] Hiroi R, Sinha Ray S, Okamoto M, Shiroi T. Macromol Rapid Commun 2004;25:1359.
[11] Sinha Ray S, Yamada K, Okamoto M, Ogami A, Ueda K. Chem Mater 2003;15:1456.
[12] Kim YH, Okamoto M, Kotaka T. Macromolecules 2000;33:8114.
[13] Tabor BJ, Marge EP, Boo J. Eur Polym J 1971;7:1127.
[14] Atkins PW. Physical chemistry. Oxford: Oxford University Press; 1998.
[15] Sinha Ray S, Yamada K, Okamoto M, Ueda K. Polymer 2003;44:857.

[16] Sinha Ray S, Okamoto K, Okamoto M. Macromolecules 2003;36:2355.
[17] Okamoto K, Sinha Ray S, Okamoto M. J Polym Sci Part B Polym Phys 2003;41:3160.
[18] Asai K, Okamoto M, in preparation.
[19] Nam PH, Maiti P, Okamoto M, Kotaka T, Hasegawa N, Usuki A. Polymer 2001;42:9633.
[20] Sinha Ray S, Maiti P, Okamoto M, Yamada K, Ueda K. Macromolecules 2002;35:3104.
[21] Sinha Ray S, Yamada K, Okamoto M, Ueda K. Polymer 2003;44:6633.
[22] Ito Y, Yamashita M, Okamoto M. Macromol Mater Eng 2006;291:773.
[23] Okamoto M, Saito T, Yoshida O, in preparation.